9. Ma X. D., Haimson B. C., Rudnicki J. W. True triaxial failure stress and failure plane of two porous sandstones subjected to two distinct loading paths. *Porous Rock Fracture Mechanics*. 2017. pp. 285–307. DOI:10.1016/B978-0-08-100781-5.00013-0
10. Ingraham M. D., Issen K. A., Holcomb D. J. Response of Castlegate sandstone to true triaxial states of stress. *Journal of Geophysical Research: Solid Earth*. 2013. Vol. 118, Iss. 2. pp. 536–552.
11. Xie H., Lu J., Li C., Li M., Gao M. Experimental study on the mechanical and failure behaviors of deep rock subjected to true triaxial stress: A review. *International Journal of Mining Science and Technology*. 2022. Vol. 32, Iss. 5. pp. 915–950.
12. Haimson B., Chang C. A new true triaxial cell for testing mechanical properties of rock, and its use to determine rock strength and deforability of Westerly granite. *International Journal of Rock Mechanics and Mining Sciences*. 2000. Vol. 37, Iss. 1–2. pp. 285–296.
13. Ma X., Rudnicki J. W., Haimson B. C. The application of a Matsuoka–Nakai–Lade–Duncan failure criterion to two porous sandstones. *International Journal of Rock Mechanics and Mining Sciences*. 2017. Vol. 92. pp. 9–18.
14. Sidorin Yu. V., Ustinov K. B., Sirotin A. A., Kovalenko Yu. F., Karev V. I. et al. Experimental investigation of deformation of rocks in plane strain and plane stress. *Processi v geosredah*. 2016. No. 2(6). pp. 148–155.
15. Rodriguez N. M., Lade P. V. True triaxial tests on cross-anisotropic deposits of fine Nevada sand. *International Journal of Geomechanics*. 2013. Vol. 13, Iss. 6. pp. 779–793. 2013.
16. Alejano L. R., Bobet A. Drucker–Prager Criterion. *Rock Mechanics and Rock Engineering*. 2012. Vol. 45. pp. 995–999.
17. Mogi K. Fracture and flow of rocks under high triaxial compression. *Journal of Geophysical Research*. 1971. Vol. 76, No. 5. pp. 1255–1269.
18. Lade P. V., ASCE AM., Musante H. M. Three-Dimensional Behavior of Remolded Clay. *Journal of the Geotechnical Engineering Division*. 1978. Vol. 104, Iss. 2.
19. Yu M. H., Zan Y. W., Zhao J., Yoshimine M. A Unified Strength criterion for rock material. *International Journal of Rock Mechanics and Mining Sciences*. 2002. Vol. 39, Iss. 8. pp. 975–989.
20. Karev V. I., Klimov D. M., Kovalenko Y. F., Ustinov K. B. Fracture of sedimentary rocks under a complex triaxial stress state. *Mechanics of Solids*. 2016. Vol. 51. No. 5. pp. 522–526.
21. Karev V. I., Khimulia V. V., Shevtsov N. I. Experimental studies of the deformation, destruction and filtration in rocks: a review. *Mechanics of Solids*. 2021. Vol. 56, No. 5. pp. 613–630.
22. Vaisberg L. A., Kameneva E. E. Loading rate effect on pore space structure in rocks. *Gornyi Zhurnal*. 2021. No. 11. pp. 17–21.
23. Viktorov S. D., Kochanov A. N. Formation of microcracks upon the dynamic fracturing of rocks. *Bulletin of the Russian Academy of Sciences: Physics*. 2015. Vol. 79, No. 6. pp. 743–745.
24. Liu K., Zhao J. Progressive damage behaviours of triaxially confined rocks under multiple dynamic loads. *Rock Mechanics and Rock Engineering*. 2021. Vol. 54. pp. 3327–3358.
25. Liu P., Liu K, Zhang QB. Experimental characterisation of mechanical behaviour of concrete-like materials under multiaxial confinement and high strain rate. *Construction and Building Materials*. 2020. Vol. 258. ID. 119638.
26. Galkin S., Savitckii I., Shustov D., Kukhtinskii A., Osovetsky B. et al. Modeling of crack development during proppant hydraulic fracturing in a clay-carbonate oil deposit. *Fluid Dynamics & Materials Processing*. 2022. Vol. 19(2). pp. 273–284.
27. Feng X. T., Kong R., Zhang X., Yang C. Experimental study of failure differences in hard rock under true triaxial compression. *Rock Mechanics and Rock Engineering*. 2019. Vol. 52. pp. 2109–2122.
28. Ma X., Haimson B. C., Rudnicki J. W. True triaxial failure stress and failure plane of two porous sandstones subjected to two distinct loading paths. *Porous Rock Fracture Mechanics*. 2017. pp. 285–307.
29. Ma X., Rudnicki J. W., Haimson B. C. Failure characteristics of two porous sandstones subjected to true triaxial stresses: applied through a novel loading path. *International Journal of Mining Science and Technology*. 2017. Vol. 122, Iss. 4. pp. 2525–2540.
30. Rudnicki J. W. Failure of rocks in the laboratory and in the Earth. *22nd International Congress of Theoretical and Applied Mechanics, Adelaide, Australia*. 2013. 199–215. pp. EM

UDC 550.348

A. Yu. MOTORIN[1,2]*, Junior Researcher, Senior Geophysicist*
S. V. BARANOV[1]*, Chief Researcher, Doctor of Physical and Mathematical Sciences, bars.vl@gmail.com*
P. N. SHEBALIN[2,3]*, Director, Doctor of Physical and Mathematical Sciences, Corresponding Member of RAS*

[1]*Kola Branch of the Geophysical Survey of the Russian Academy of Sciences, Apatity, Russia*
[2]*Kirovsk Branch of Apatit, Kirovsk, Russia*
[3]*Institute of Earthquake Prediction Theory and Mathematical Geophysics, Russian Academy of Sciences, Moscow, Russia*

SPATIAL DISTRIBUTION OF BLAST-TRIGGERED SEISMIC EVENTS: A CASE-STUDY OF THE KHIBINY MASSIF

The paper considers spatial distribution of seismic events triggered by blasts during mineral mining in the Khibiny Massif. The subject of the study is the production blasts and seismic events recorded by the seismic monitoring network of Kirovsk Branch of Apatit in 1996–2020. The chains of seismic events triggered by blasts were identified using the nearest-neighbor method. The studies prove that earthquake-to-blast distances averagely obey an exponential distribution independent of the triggering blast magnitudes. The model of the maximal distances from a triggering blast hypocenter to the expected aftershocks with a given probability is constructed in the study. The model agrees with the actual data. The recommendations on using the mode are substantiated from the analysis of the error diagrams.

Keywords: *induced seismicity, production blasts, aftershocks, exponential distribution, aftershock domain, error diagram*
DOI: *10.17580/em.2023.02.07*

Introduction

This study continues the research of the authors in the field of time–space patterns of seismic activity in the regions of mineral mining. It is already demonstrated that the number of seismic events triggered by blasting (seismic productivity of blasts) obeys an exponential distribution [1]. It is also found that under conditions of the induced seismicity in the Khibiny Massif, the distances between the seismic events and induced bumps comply with a power-series distribution [2]. A similar result was earlier obtained by the American scientists for the natural seismicity in California [3]. Using the combination of the earthquake productivity law [4], proved for the conditions of the induced seismicity in the

Khibiny [5], and the power-series distribution of distances [2], the distribution of maximal distances between the triggering seismic events and the induced bumps was derived. This study analyzes features of the spatial distribution of seismic events triggered by blasting at the mineral deposits of the Khibiny Massif.

The Khibiny Massif in the west of the Kola Peninsula is the largest alkaline intrusion in the world. The southwestern area of the Massif comprises large apatite–nepheline deposits (Kukisvumchorr, Yuksporr, Apatite Circus and Rasvumchorr Plateau). They have been developed by Kirovsk Branch of Apatit for more than 80 years and representing different parts of the same apatite–nepheline body [6]. The depth of the deposits reaches 1.5 km, and the thickness is 0.5 km. Alongside with the high tectonic stresses of up to 40–60 MPa at the depth of 0.2–0.6 km below ground surface, which sometimes exceed the gravitational stresses by an order of magnitude [7], the Massif contains numerous faults, some of them intersecting the deposits [8]. The recent uplifting events at a rate from 0.5 to 2–4 mm per year in the Khibiny Massif, as well as the periodic earthquakes [9] reflect of the modern tectonic evolution in the region. Seismicity in the Khibiny is a result of the joint influence of tectonics and mining activity.

The impact of blasting on the energy of seismic events is comprehensively considered in the studies [10–12]. Blasts violate the local stress field near a hypocenter and generate stress concentrate zones, which leads to brittle fracture of rock mass (induced seismicity). Although blasting-induced seismic events are small as compared to the natural seismicity [12], they can endanger mining operations [13, 14].

After blasting, in a certain neighborhood of a blast, a short-term increase in the seismic activity is often observed (post-blasting seismicity), similarly to the main shock–aftershock pattern, a blast plays the part of the main shock or trigger [10, 15, 16]. For estimating this neighborhood, it is required to understand how the post-blast seismicity attenuates with the distance from the trigger blast. This can enable estimating future post-blast seismicity region at the blasting design stage, and making provisions to ensure safety of personnel and machinery. This is the subject of this paper.

The tasks solved in this study include: 1) the analysis of distribution of distances from trigger blast to seismic events triggered by them; 2) determination of the maximal distance distribution based on the law of seismic productivity of blasts; 3) the modeling of the post-blasting seismicity with practical guidelines on the model application in the conditions of induced seismicity in the Khibiny Massif. The proposed model allows sizing up a zone of expected triggerd events at a preset accuracy. We emphasize that this result is critical for the mining safety.

Initial data and identification of triggered events

As in [1], this study used the catalog of seismic events recorded by the seismic monitoring network of Kirovsk Branch of Apatit [17] from 1996 to 2020, Nowadays the network contains 65 three-component seismic sensors with the sampling frequency of 1000 Hz arranged in Kirovsky and Rasvumchorr Mines. Monitoring enables positioning of hypocenters of seismic events having the energy $E \geq 10^4$ J at an accuracy to 25 m in the confident recording region. Processing of the seismic monitoring data at Kirovsk Branch of Apatit included calculation of the seismic event energy E, J. In this study, the energy conversion in the magnitude used Rautian's formula $\lg E(\mathrm{J}) = 1.8M + 4.0$ [18]. Starting from 1996, the representative network energy $E_{rn} = 10^4$ J, which complies with the representative magnitude $M_{rn} = 0$. The catalog used in this study contained data on 71664 seismic events having $0 \leq M \leq 3.3$.

The spatial distribution analysis of seismic events triggered by blasting used the catalog of blasts implemented at apatite–nepheline deposits in the Khibiny Massif during the selected span.

The chains of trigger blasts and seismic events triggered by them were identified using the nearest neighbor algorithm [19, 20]. In this algorithm, for each catalogued earthquake, a foregoer is found amongst all preceding blasts by the criterion of the minimum proximity function in the space–time–magnitude (energy) environment. This method of identifying seismic events induced by basting in the Khibiny Massif is described in [1].

Distribution of distances from trigger blasts to trigger events

In the framework of this study, distribution of the epicentral distances r from the trigger blasts with the magnitudes $M_m \geq 2$, $M_m \geq 2.2$ and $M_m \geq 2.4$ to induced events with the magnitudes $M \geq M_m$–1.5 is plotted (**Fig. 1**). It appears that for the post-blasting seismicity in the Khibiny Massif, these distances starting from the value r_0 follow the exponential distribution function:

$$F_r(x) = P(r < x) = 1 - e^{-s(x-r_0)}, \quad x \geq r_0 \tag{1}$$

at PDF:

$$f_r(x) = P(r < x) = se^{-s(x-r_0)}, \quad x \geq r_0 \tag{2}$$

According to the method of maximum similarity, the estimate $1/s$ is an average value of r–r_0 when $r \geq r_0$; the value r_0 is found from the Goodness-of-Fit test [21]; σ is evaluated using bootstrap. The evaluated parameter s, standard error σ (for s) and r_0 are given in the caption for Fig. 1. The same distribution, starting from a certain value of h_0, is valid for the distances in depth (**Fig. 2**).

For different magnitudes M_m of a trigger blast, the scatter of s is lower than the standard error of both epicentral distances (see fig. 1) and depth-wise distances (see fig. 2). We should mention that for the depth-wise distances, the scatters of the parameter s and standard error σ for different magnitudes are higher than for the epicentral distances. This is connected with the higher errors in the determination of depths than epicenters, and, probably with the depth-wise nonuniformity of the stress fields, which increase probability of dynamic events triggered due to rock pressure [22, 23], which may lead to variations in the depth-wise decrease in the number of triggered events characterized by the parameter s. In any case, for the epicentral distances (see fig. 1) and depth-wise distances (see fig. 2), the scatter of the estimated values of s falls within a proper interval of $\pm\sigma$ for $M_m \geq 2$, which reflects of insignificant discrepancy in the parametrs values. Similarly the parameter s is independent of the magnitude of a trigger blast. The situation the same with the post-seismic activity at the Khibiny deposits [2].

It is shown in [2] that attenuation of the post-seismic activity (seismic events triggered by an earlier earthquake) in the Khibiny Massif obeys an exponential law. This means that the post-blasting seismicity attenuates faster than the post-seismic activity. This fact is naturally explained by the fact that an earthquake–trigger occurs in a certain neighborhood of a hypocenter at a certain level of stresses. The jump in the stresses under that trigger and their further relaxation initiates aftershocks [24]. The same mechanism is valid for the trigger events triggered by blasts [10, 12, 15]. Blasts have no directivity patterns and occur irrespective of the stress level. Therefore, blast triggered events are fewer [1] and their number decays faster as the distance increases from the trigger compared to the case when the trigger is a seismic event.

Model of the aftershock domain

Since the parameter s of exponential distribution (1) is independent of the magnitude of a trigger blast, the radius R of a circle embracing expected induced events with the magnitude $M \geq M_m$–ΔM is governed by the number of the induced events of the preset magnitude (seismic productivity of a blast).

A triggering blast can initiate a few blast-dependent events that make a series. In our study, we consider a single hierarchy scale, and we assume that the events in the series are independent of each other, and in each series, the number of the blast-triggered events with the magnitudes $M_m \geq 2$ to the earthquake-triggered events with $M \geq M_m$–1.5 obey the Poisson distribution with an average Λ [25]. In this case, the probability that all triggered events k take place at a distance less than x from a trigger is $F_r(x)^k$, where $F_r(x)$ is distribution (1). Using the formula of total

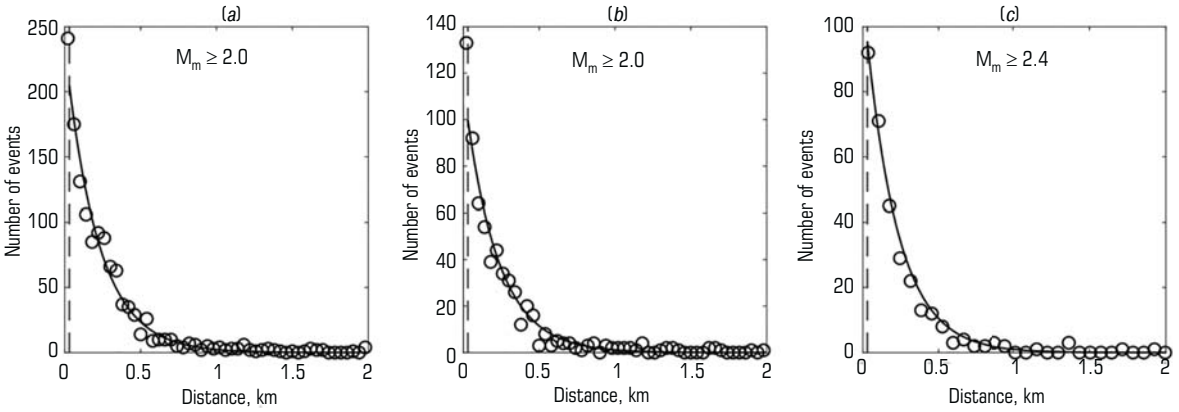

Fig. 1. Distribution of epicentral distances from trigger blastswith different magnitudes M_m to triggered seismic events with $M \geq M_m$–1.5 (circles—actual values; solid line—approximation by exponential distribution (2); dashed line corresponds to r_0, wherefrom the distances obey exponential distribution): *a* – $M_m \geq 2.0$, $r_0 = 0.03$ km, $s = 4.61$, $\sigma = 0.14$ (standard error); *b* – $M_m \geq 2.2$, $r_0 = 0.03$ km, $s = 4.60$, $\sigma = 0.20$; *c* – $M_m \geq 2.4$, $r_0 = 0.03$ km, $s = 4.71$, $\sigma = 0.28$ (values of r_0 exceed hypocenter identification accuracy of 0.025 km)

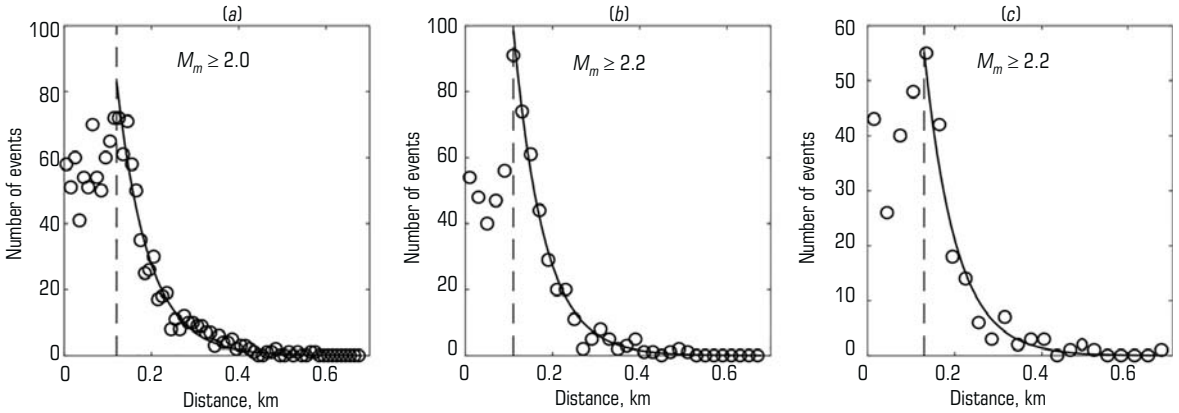

Fig. 2. Depth-wise distribution of distances from trigger blasts with different magnitudes M_m to triggered events seismic events with $M \geq M_m$–1.5 (circles—actual values; solid line—approximation by exponential distribution (2); dashed lines corresponds to h_0, starting from which the distances obey exponential distribution): *a*–$M_m \geq 2.0$, $h_0 = 0.12$ km, $s = 13.78$, $\sigma = 0.56$ (standard error); *b*–$M_m \geq 2.2$, $h_0 = 0.11$ km, $s = 14.30$, $\sigma = 0.77$; *c*–$M_m \geq 2.4$, $h_0 = 0.13$ km, $s = 13.73$, $\sigma = 1.19$ (values of h_0 exceed hypocenter identification accuracy of 0.025 km)

probability, we obtain a distribution of the maximal epicentral distance R_{max} from a trigger blast to a most remote aftershock in a series:

$$F_\Lambda(x) = P(R_{\max} < x) = \sum_{k=0}^{\infty} F_r(x)^k \frac{\Lambda^k}{k!} e^{-\Lambda} = e^{-\Lambda[1-F_r(x)]},\ x \geq r_0. \quad (3)$$

By the law of seismic productivity of blasts [1], the number of the blast-induced events obeys the exponential distribution with a frequency:

$$f_{ex}(\Lambda) = \frac{1}{L} e^{-\Lambda/L}. \quad (4)$$

Here, the parameter L is an average number of events with $M \geq M_m$–1.5 triggered by blasts with $M_m \geq 2$.

To determine the distance distribution from the triggered events to their trigger by a set of series, we combine (3) and (4) at $x \geq r_0$. The resultant distribution function is:

$$F_a(x) = \int_0^\infty F_\Lambda(x) f_{ex}(\Lambda) d\Lambda = \frac{1}{L}\int_0^\infty e^{-\Lambda/L} e^{-\Lambda[1-F_r(x)]} d\Lambda = \\ = \frac{1}{1 + Le^{-s(x-r_0)}},\ x \geq r_0. \quad (5)$$

at the frequency:

$$F_a'(x) = f_a(x) = \frac{Lse^{-s(x-r_0)}}{\left[1 + Le^{-s(x-r_0)}\right]^2},\ x \geq r_0, \quad (6)$$

where F_r is the function of exponential distribution (1); f_r is its frequency (2).

The analogous expressions are valid for the distances in depth at a difference that r_0 (epicentral distance starting from which the number of the blast-induced events reduces exponentially) should be substituted for h_0 (depth-wise distance starting from which the number of the blast-triggered events reduces exponentially).

The agreement of distribution frequency (6) and the actual seismicity in the Khibiny Massif is illustrated in **Fig. 3**. The value $L = 0.64$ is calculated using [1], where the following estimates are obtained: the parameter of distribution of seismic event magnitudes (frequency curve slope)—$b = 1.25$, average number of seismic events with $M \geq M_m$–2 triggered by blasts with c $M_m \geq 2$—$\Lambda_2 = 2.7$. Then, by the Guttenberg–Richter law, using the legend from [1], $\Lambda_{1.5} = \Lambda_2 10^{b(1.5-2)} = = 0.64 = L$.

Practical use

It is difficult to apply the distribution (5) to determine domains of the expected triggered events with the magnitudes $M \geq M_m$–1.5 at a preset probability, since as the exponential downturn only appears at a certain,

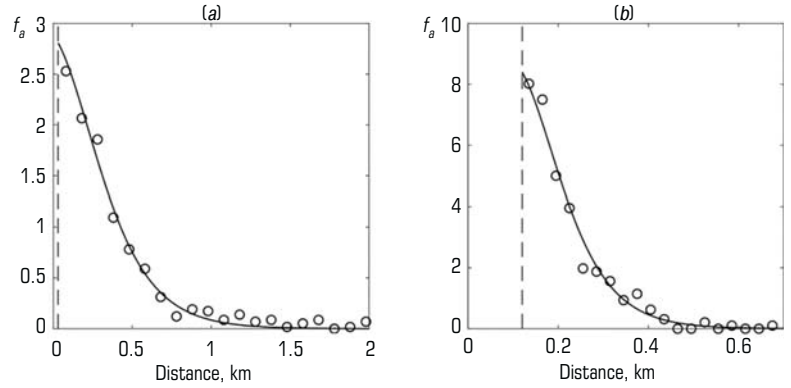

Fig. 3. Probability density of maximal epicentral distances R_{max}, km (*a*) and depth-wise distances H_{max}, km (*b*) from blasts–trigger with $M_m \geq 2$ to triggered events with $M \geq M_m$–1.5. Circles–actual data; solid line–approximation by (6)

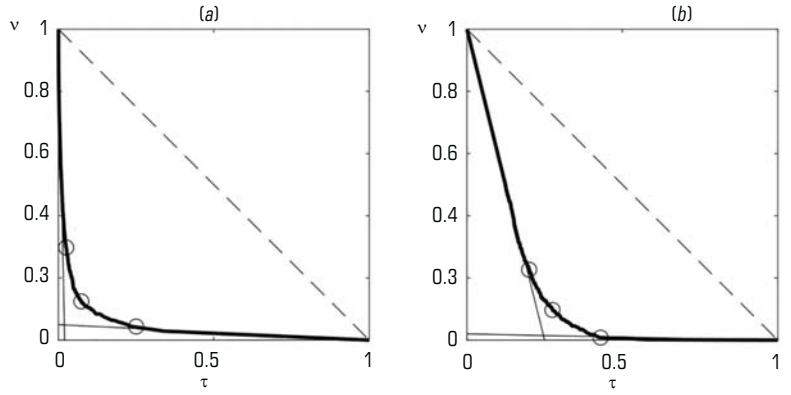

Fig. 4. Error diagram for distances: epicentral (a) and depth-wise (b) distances from trigger blast with $M_m \geq 2$ tor the farthest shock with $M \geq M_m$–1.5:
τ–alarm rate; ν–detecting failure rate. Dashed line–diagonal (0.1)–(1.0) of random prediction; heavy line–error path; circles (0), (1) and (2) of neutral, soft and hard-line prediction strategies, respectively (congruent values of ν and τ are compiled in the Table below); fine lines–tangents to error path at points 1 and 2 (tangent to point 2 in (*b*) coincides with abscissa axis)

The trigger blast parameters q, ν, τ, R_{max} and H_{max} to fit with different prediction strategies

Strategy	q	τ	ν	R_{max}, km
	Epicentral estimates			
Neutral	0.97	0.08	0.12	0.69
Soft	0.89	0.03	0.30	0.40
Hard-line	0.99	0.24	0.04	1.2
	Depth-wise estimates			H_{max}, km
Neutral	0.94	0.28	0.10	0.28
Soft	0.84	0.22	0.23	0.20
Hard-line	0.99	0.43	0.01	0.43

though short, distance from a trigger blast, and about 25% of all triggered events occur at this distance. To consider this feature the constrained mining area we use Molchan's error diagram [26] which shows a detecting failure rate ν versus an alarm rate τ.

Similarly to [2], in the assessment of epicentral distances beyond the domain Ω embracing 100% of aftershocks, the circle radius was assumed to be equal to 2.5 km with the center in the epicenter of a trigger blast. Such Ω conforms with the control zone of the Joint Kirov Mine. The estimate of the epicentral alarm domain where aftershocks were expected was assumed as a circle with the center in the trigger blast epicenter and the radius R_q calculated for the inverse function probability q for distribution (6): $R_q = F_a^{-1}(q)$. For the trigger blasts with $M_m \geq 2$, the parameters included in distribution (5) are: $s = 4.61$, $r_0 = 0.03$ km (Fig. 1, *a*), $L = 0.64$. This domain is denoted by G_q, and its area is S_q. The alarm rate τ was found as a ratio of S_q to the area of Ω (parameter S_Ω), i.e. $\tau = S_q/S_\Omega$. The detecting failure rate ν is a percentage of aftershocks beyond the alarm domain G_q.

In the depth-wise assessment, the domain Ω was assumed to be a domain with the length $H_\Omega = 1$ km, with the center in the trigger blast hypocenter, which agreed with the depth-wise control zone in mines, and enabled encompassing 100% of aftershocks. The depth-wise alarm domain of expected triggered events was assumed to be a vertical domain V_q with the center in the trigger blast hypocenter, and with the length H_q calculated for the inverse probability function q for the depth-wise frequency F_a (6). For the trigger blasts, the parameters in distribution (5) are: $s = 13.78$, $h_0 = 0.12$ km (see fig. 2, *a*), $L = 0.64$. In this case, the alarm rate $\tau = H_q/H_\Omega$. The detecting failure rate ν is a rate of aftershocks beyond the domain V_q.

Such shape of the domain conforms with a cylinder with the radius R_q and the height H_q, and the center of the cylinder coincides with the epicenter of a trigger blast. The choice of such shape of the domain allows determining the radius and height of the cylinder independently, based on the sensitivity of the prediction.

The ν / τ ratio for different q is an error path. The diagonal (0; 1) (1; 0) stands for the random prediction. A stronger deviation of the error path from this diagonal means a better prediction. The parameter q sets the size of the alarm domain: the higher q defines the large domain G_q or V_q.

The error diagram plotted for different q by the retrospective prediction of a domain of aftershocks with $M \geq M_m$–1.5 (**Fig. 4**) represents a compromise between the errors of two kinds: an increase in q decreases probability of detecting failure by increases the alarm domain, and vice versa. Thus, the scalar parameter q may be described as an *alarm function* [27].

Evidently, the choice of the value of q should depend on the objectives of the prediction. Sometimes, it is important to have a low probability of the error of the second kind, i.e. detecting failure, for instance, when an aftershock may lead to unwanted consequences. In other case, it may be required to minimizes the size of the domain of expected aftershocks, to reduce the cost of alarm maintenance. For the standardized selection of q, the three strategies method was proposed [28]. The method consists in determining limit points in the error path, to math with the neutral soft and hard-line strategies (see fig. 4).

The neutral strategy point (point 0 in fig. 4) is identified by the criterion of the minimum loss function $\gamma = \nu + \tau$, which is a sum of errors of two kinds. This strategy is applied when costs of errors of two kinds are nearly the same or unknown. The soft strategy point (point 1 in fig. 4) is governed by the position of a tangent to the error path, where due to the proximity of the path to a vertical line even a small change in size of the alarm domain by reduction in q, can lead to a high rise in the detecting failure probability. Finally, the hard-line strategy is point 2 in Fig. 4; the tangent to the error path at this point means that the enlargement of the alarm domain cannot reduce the failure rate because of the closeness of the path to a horizontal line.

The **Table** compiles the values of the trigger blast parameters q, ν, τ, R_{max} and H_{max} to fit with the neutral, soft and hard-line strategies.

When estimating domains of aftershocks triggered by trigger blasts at the Khibiny deposits, these tabulated data may be used as a first approximation at the blasting design stage. The independence of the epicentral

and depth-wise estimates allows using different strategies of choosing the radius and height of a cylindrical domain subject to a blast location.

For more accurate evaluation for a specific series, it is required to take into account the information of the first aftershocks. The model described in this article is applicable as a reference model in testing models of the first aftershocks. The case-study of the reference model application in the assessment of a strong aftershock magnitude and the hazardous period duration is presented in [29].

Conclusions

Based on the evidence of long-term data on seismicity and blasting operations in the Khibiny Massif, it has been shown that the distances from the trigger blasts to the shocks triggered by them averagely obey the exponential distribution almost independent of the magnitude of a trigger blast. Unlike aftershocks triggered by earthquakes (exponential law-based attenuation), the blast-induced events attenuate faster since an earthquake, as against a blast, occurs when rocks have accumulated a certain level of stresses.

The analytical research produced a distribution of the maximal distances at which the post-blasting seismicity is expected, using the law of seismic productivity of blasts and the exponential attenuation of the post-blast seismicity with an increasing distance (epicentral and depth-wise). The complience of the distribution and actual data is demonstrated.

The authors propose modeling the post-blast seismicity domain as a cylinder with the center in the epicenter of a trigger blast. The radius and height of the cylinder are determined depending on the prediction, importance based on analysis of an error diagram. The model provides statistically valid estimates at the stage of the blast design.

Acknowledgements

The study includes results obtained under the state contract between the Ministry of Science and Higher Education of the Russian Federation and the Geophysical Survey of the Russian Academy of Sciences, Contract No. 075-01471-22.

References

1. Baranov S. V., Zhukova S. A., Korchak P. A., Shebalin P. N. Seismic productivity of blasts: A case-study of the Khibiny Massif. *Eurasian Mining*. 2020. No. 2. pp. 14–18.
2. Baranov S. V., Motorin A. Yu., Shebalin P. N. Spatial distribution of triggered earthquakes in the conditions of mining-induced seismicity. *Izvestiya. Physics of the Solid Earth*. 2021. Vol. 57, No. 4. pp. 520–528.
3. Felzer K. R., Brodsky E. E. Decay of aftershock density with distance indicates triggering by dynamic stress. *Nature*. 2006. Vol. 441, No. 7094. pp. 735–738.
4. Shebalin P. N., Narteau C., Baranov S. V. Earthquake productivity law. *Geophysical Journal International*. 2020. Vol. 222, Iss. 2. pp. 1264–1269.
5. Baranov S. V., Zhukova S. A., Korchak P. A., Shebalin P. N. Productivity of mining-induced seismicity. *Izvestiya. Physics of the Solid Earth*. 2020. Vol. 56, Iss. 3. pp. 326–336.
6. Nivin V. A. Occurrence forms, composition, distribution, origin and potential hazard of natural hydrogen-hydrocarbon gases in ore deposits of the Khibiny and Lovozero Massifs: A Review. *Minerals*. 2019. Vol. 9, Iss. 9. DOI: 10.3390/min9090535
7. Rebetsky Yu. L., Sim L. A., Kozyrev A. A. Possible mechanism of horizontal overpressure generation of the Khibiny, Lovozero, and Kovdor Ore Clusters on the Kola Peninsula. *Geology of Ore Deposits*. 2017. Vol. 59. pp. 265–280.
8. Shabarov A. N., Kuranov A. D. Kiselev V. A. Assessing the zones of tectonic fault influence on dynamic rock pressure manifestation at Khibiny deposits of apatite-nepheline ores. *Eurasian Mining*. 2021. No. 2. pp. 3–7.
9. Kremenetskaya E. O., Trjapitsin V. M. Induced seismicity in the Khibiny Massif (Kola Peninsula). *Pure and Applied Geophysics*. 1995. Vol. 145. pp. 29–37.
10. Adushkin V. V., Spivak A. A. Geomechanics of Large-Scale Blasts. Moscow : Nedra, 1993. 319 p.
11. Adushkin V. V. Blasting-induced seismicity in the European part of Russia. *Izvestiya. Physics of the Solid Earth. 2013*. Vol. 49. pp. 258–277.
12. Kocharyan G. G., Kulikov V. I., Pavlov D. V. Impact of massive blasts on stability of tectonic faults. *Journal of Mining Science*. 2019. Vol. 55, No. 6. pp. 905–913.
13. Kozyrev A. A., Semenova I. E., Zhuravleva O. G., Panteleev A. V. hypothesis of strong seismic event origin in Rasvumchorr mine on January 9, 2018. *GIAB*. 2018. No. 12. pp. 74–83.
14. Gospodinov D., Dineva S., Dahnér-Lindkvist C. On the applicability of the RETAS model for forecasting aftershock probability in underground mines (Kiirunavaara Mine, Sweden). *Journal of Seismology*. 2020. Vol. 26. pp. 1023–1037.
15. Woodward K., Wesseloo J. Observed spatial and temporal behaviour of seismic rock mass response to blasting. *Journal of the Southern African Institute of Mining and Metallurgy*. 2015. Vol. 115, Iss. 11. pp. 1045–1056.
16. Dokht R. M. H., Smith B., Kao H., Visser R., Hutchinson J. Reactivation of an intraplate fault by mine-blasting events: Implications to regional seismic hazard in Western Canada. *Journal of Geophysical Research: Solid Earth*. 2020. Vol. 125, Iss. 6. DOI: 10.1029/2020JB019
17. Korchak P. A.., Zhukova S. A., Menshikov P. Yu. Seismic monitoring build-up and development in the production activity zone of Apatit JSC. *Gornyi Zhurnal*. 2014. No. 10. pp. 42–46.
18. Rautian T. G. Earthquake Energy. Seismic Survey Methods. Moscow : AN SSSR, 1960. pp. 75–114.
19. Zaliapin I., Ben-Zion Y. Earthquake declustering using the nearest-neighbor approach in space-time-magnitude domain. *Journal of Geophysical Research: Solid Earth*. 2020. Vol. 125, Iss. 4. DOI: 10.1029/2018JB017120
20. Bayliss K., Naylor M., Main I. G. Probabilistic identification of earthquake clusters using rescaled nearest neighbor distance networks. *Geophysical Journal International*. 2019. Vol. 217, Iss. 1. pp. 487–503.
21. Wiemer S., Wyss M. Minimum magnitude of complete reporting in earthquake catalogs: examples from Alaska, the Western United States, and Japan. *Bulletin of the Seismological Society of America*. 2000. Vol. 90, Iss. 4. pp. 859–869.
22. Sinegubov V. Yu., Maksimov A. B., Streletskyi A. V. Ivanov Yu. S. Mining Safety under Conditions of Rockburst Hazard (Underground Mining at Apatite–Nepheline Deposits of Kirovsk Branch of Apatit: Kukisvumchorr, Yukspor, Apatite Circus, Rasvumchorr Plateau): Guidance. Kirovsk : Teleset, 2021. 96 p.
23. Kozyrev A. A., Panin V. I., Semenova I. E., Rybin V. V. Geomechanical support of mining operations in mines of the Murmansk Region. *Gornyi Zhurnal*. 2019. No. 6. pp. 45–50.
24. Smirnov V. B., Ponomarev A. V. Physics of Transient Seismic Modes. Moscow : RAS, 2020. 412 p.
25. Shcherbakov R., Zhuang J., Ogata Y. Constraining the magnitude of the largest event in a foreshock–main shock–aftershock sequence. *Geophysical Journal International*. 2018. Vol. 212, Iss. 1. pp. 1–13.
26. Molchan G. Space–time earthquake prediction: The error diagrams. *Pure and Applied Geophysics*. 2010. Vol. 167. DOI: 10.1007/s00024-010-0087-z
27. Zechar J. D., Jordan T. H. Testing alarm-based earthquake predictions. *Geophysical Journal International*. 2008. Vol. 172, Iss. 2. pp. 715–724.
28. Baranov S. V., Shebalin P. N. Forecasting aftershock activity: 2. Estimating the area prone to strong aftershocks. *Izvestiya, Physics of the Solid Earth*. 2017. Vol. 53. pp. 366–384.
29. Baranov S., Narteau C., Shebalin P. Modeling and prediction of aftershock activity. *Surveys in Geophysics*. 2022. Vol. 43. pp. 437–481. EM